frontiers | Frontiers in Earth Science

TYPE Original Research
PUBLISHED 08 April 2024
DOI 10.3389/feart.2024.1272857

OPEN ACCESS

EDITED BY
Omid Haeri-Ardakani,
Department of Natural Resources, Canada

REVIEWED BY
Ali Kadkhodaie,
University of Tabriz, Iran
Salvatore Magazù,
Università di Messina, Italy

*CORRESPONDENCE
He Huang,
huanghe@cdut.edu.cn

RECEIVED 04 August 2023
ACCEPTED 18 March 2024
PUBLISHED 08 April 2024

CITATION
Li Y, Huang H, Gao Y, Cao Y, Cheng H, Hei C and Liang S (2024), The ~170 kyr astronomical cycle in the Early Permian Lucaogou Formation of the Junggar Basin.
Front. Earth Sci. 12:1272857.
doi: 10.3389/feart.2024.1272857

The ~170 kyr astronomical cycle in the Early Permian Lucaogou Formation of the Junggar Basin

Yuyin Li[1,2,3], He Huang[1,2]*, Yuan Gao[3,4], Yongqiang Cao[5], Hu Cheng[3], Chenlu Hei[3] and Shuang Liang[3]

[1]State Key Laboratory of Oil and Gas Reservoir Geology and Exploitation, Institute of Sedimentary Geology, Chengdu University of Technology, Chengdu, China, [2]Key Laboratory of Deep-time Geography and Environment Reconstruction and Applications of Ministry of Natural Resources, Chengdu University of Technology, Chengdu, China, [3]School of Earth Sciences and Resources, China University of Geosciences (Beijing), Beijing, China, [4]State Key Laboratory of Biogeology and Environmental Geology, China University of Geosciences (Beijing), Beijing, China, [5]Fourth Geological Brigade of North China Geological Exploration Bureau, Tianjin North China Geological Exploration Bureau, Qinhuangdao, China

According to Milankovitch's theory, periodic climate change in Earth's history is controlled by the periodic changes in the Earth's orbit and axis of rotation. Milankovitch cycle include eccentricity, obliquity, and precession cycles. In addition to them, there are also some amplitude modulation (AM) cycles that affect the climate system through a series of "nonlinear" feedback processes, such as the 173 kyr obliquity AM cycle. Previous studies have demonstrated that the ~170 kyr cycle modulate the paleoclimate and carbon cycle at mid-high latitude regions in the Meso-Cenozoic. However, due to the limitation of astronomical solutions and the lack of high-resolution geological records, the ~170 kyr cycle has been less reported in the Paleozoic Era. In this study, cyclostratigraphic analysis of natural gamma ray (GR) logging data from four wells (Ji30, Ji31, Ji32, and Ji174) and total organic carbon (TOC) data from well Ji174 penetrating the Early Permian Lucaogou Formation in Jimusar Sag, Junggar Basin suggests preservation of eccentricity, obliquity, and precession cycles, and the ~170 kyr AM cycle. Through the astronomical tuning of GR logging data obtained from four wells to eccentricity target cycles, we established the floating astronomical time scale (ATS). The results indicate an average sedimentation rate ranging from 7.4 to 9.5 cm/kyr and a duration from 2.8 to 3.2 million years (Myr) for the Lucaogou Formation. The differences in sedimentation rate and duration among these four wells may result from different well locations. Moreover, the ~170 kyr cycle signal has been identified in the detrended GR logging and TOC data series, and its obliquity AM series. This signal might be attributed to the obliquity AM cycles originated from the interaction between s_3 and s_6 (s_3 and s_6 represent the precession of nodes of Earth and Saturn), which was recorded in the GR logging and TOC data time series due to nonlinear responses within the depositional system.

KEYWORDS

cyclostratigraphy, Milankovitch cycle, paleoclimate, organic carbon burial, Permian, Lucaogou Formation

1 Introduction

The periodic variations in Earth's orbital parameters, including eccentricity, obliquity and precession, induce changes in the Earth's climate system, affecting sedimentary processes and leaving periodic imprints in sedimentary records (Hinnov, 2000; Wu et al., 2011; Tian et al., 2022). These cycles, known as Milankovitch cycles or astronomical cycles, influence the Earth's climate system on timescales ranging from millions to thousands of years. Conventionally, the astronomical cycles include eccentricity cycles of ~405 kyr and ~100 kyr, an average obliquity cycle of ~40 kyr, and an average precession cycle of ~20 kyr at present day. In addition to these astronomical cycles, some studies have gradually revealed amplitude modulation (AM) cycles of the eccentricity and obliquity cycles (Huang et al., 2021; Zhang R. et al., 2022; Wei et al., 2023). For example, AM cycles of ~2.4 Myr have been identified in the eccentricity signals, while the amplitude curves of obliquity exhibit modulation cycles of ~1.2 Myr and ~173 kyr (Hinnov, 2000; Boulila et al., 2018; Fang et al., 2019; Ma et al., 2019; Huang et al., 2021). These AM cycles also have been demonstrated to regulate the Earth's climate, hydrological cycle, atmospheric circulation, and carbon cycle systems (e.g., Huang et al., 2020; Huang et al., 2021).

The obliquity signal influences the climate of mid-high latitude regions by affecting the latitudinal distribution of global insolation, which could leave corresponding imprints in the carbon cycle (Raymo and Nisancioglu, 2003; Huang et al., 2021). Additionally, Bosmans et al. (2015) propose that the obliquity signal can directly impact the climate of low latitude regions by influencing the meridional gradient of incoming solar radiation (Bosmans et al., 2015). For mid-high latitude regions, as the obliquity increase, the amount of solar radiation received in summer also increases. This leads to an increase in terrestrial precipitation, weathering and groundwater storage, and a decrease in sea level (Wang et al., 2020; Zhang Z. et al., 2022).

Hinnov (2000) proposed the ~170 kyr cycle firstly by obtained the theoretical obliquity series within 10 Ma. The spectral analysis of the obliquity AM series revealed not only the modulation cycle of ~1.2 Myr but also a shorter cycle of 174 kyr. In recent years, with advancements in dating techniques and the acquisition of continuous high-resolution geological records, an increasing number of studies have reported the existence of the ~170 kyr cycle. Boulila et al. (2018) found ~173 kyr signal in Eocene marine strata. After testing that the ~170 kyr cycle is reliable within 50 Ma, an ATS was established to solve the "Eocene astronomical timescale gap" problem. Charbonnier et al. (2018) captured the ~173 kyr signal in the Cretaceous marine strata and extended the reliability of the ~173 kyr signal to 100 Ma by astronomical testing, and then used the ~173 kyr cycle to establish an ATS and estimate the duration of OAE2 (Oceanic Anoxic Event 2).

For terrestrial strata, Huang et al. (2021) discovered the presence of the ~170 kyr cycle in data series from the Late Cretaceous Songliao Basin, Late Miocene Tarim Basin, and the Pliocene to Holocene Lake El'gygytgyn. Interestingly, this cycle was found not only in the TOC-derived obliquity AM series but also in the detrended TOC data series. Zhang R. et al. (2022) identified the ~173 kyr cycle in magnetic susceptibility (MS) data from aeolian loess profiles in the eastern Loess Plateau during the Late Miocene to Pliocene and attributed it to the orbital interaction between the Earth and Saturn. Furthermore, Huang et al. (2021) summarized high-resolution TOC and organic carbon isotope data from mid-high latitude regions within 200 Ma as the record of Earth's carbon cycle, revealing a cycle at 200–160 kyr. Based on these findings, they proposed the "obliquity threshold response model," suggesting that the ~170 kyr AM cycle impacts the Earth's climate system through "nonlinear" sedimentary processes, thus regulating the Earth's carbon cycle. This "nonlinear" feature and threshold responce has also been demonstrated in climate models (e.g., stochastic climate models and parametric climate models) and numerical simulation works (Caccamo and Magazù, 2021; Caccamo and Magazù, 2023). However, the specific mechanisms of how the 173 kyr obliquity AM cycle influences Earth's climate are still not fully understood, especially for the old strata beyond Mesozoic Era.

Studies on cyclostratigraphy in Paleozoic marine strata have mainly focused on eccentricity, obliquity and precession cycles (Gambacorta et al., 2018; Yao and Hinnov, 2019; Fang et al., 2020; Ma et al., 2020), with research on AM cycles mainly emphasizing the long AM cycles (e.g., 2.4 Myr, 1.2 Myr, etc.) and their impact on climate and abrupt events (Fang et al., 2018; Wu et al., 2018; Fang et al., 2019; Sørensen et al., 2020; Zhang R. et al., 2022; Zhao et al., 2022). In comparison, there are few reports on the shorter ~170 kyr AM cycle without detailed discussion (Ma et al., 2016; Huang et al., 2020). In this study, we conducted cyclostratigraphic research using natural gamma ray (GR) logging data series from four wells (Ji30, Ji31, Ji32, and Ji174) and one TOC data series (Ji174) in the Early Permian Lucaogou Formation of the Junggar Basin. We consistently identified the ~170 kyr astronomical cycle in all four wells. This signal was observed not only in the AM series of obliquity but also in detrended GR logging and TOC data series. These findings provide evidence for the existence of the ~170 kyr cycle in Paleozoic terrestrial basin. Moreover, the ~170 kyr cycle, along with the eccentricity cycles, regulates climate and hydrological cycle in mid-high latitude regions through linear and nonlinear processes, which further influences the carbon cycle.

2 Geological setting

The Junggar Basin is located in northwestern China, with an area of approximately 1.3×10^5 km^2, and it roughly has a triangular shape (Figure 1B) (Bian et al., 2010). The northeastern part is bordered by the Qinggelidi and Kelameili Mountains, while the northwestern part is adjacent to the Zhayier and Haalate Mountains (Bian et al., 2010). In the south, it extends to the Yilinheibiergen and the Bogeda Mountains. Based on the characteristics of the stratigraphic development, the basin can be divided into three stratigraphic zones and seven secondary tectonic units, which are: the northwestern zone (the Wulungu Depression, the Luliang Uplift, the Central Depression and the West Uplift), the eastern zone (the Jimusaer Sag and the East Uplift), and the southern zone (the North Margin Piedmont Thrust Zone) (Figure 1B) (Gao et al., 2020). The Junggar Basin has a complete sedimentary sequence from the Carboniferous to the Quaternary, making it one of the few well-preserved sedimentary basins in Central Asia that spans from the Late Paleozoic to Cenozoic (Carroll and Wartes, 2003). This continuous record provides excellent geological archives for conducting studies on paleoclimate and paleoenvironment. From

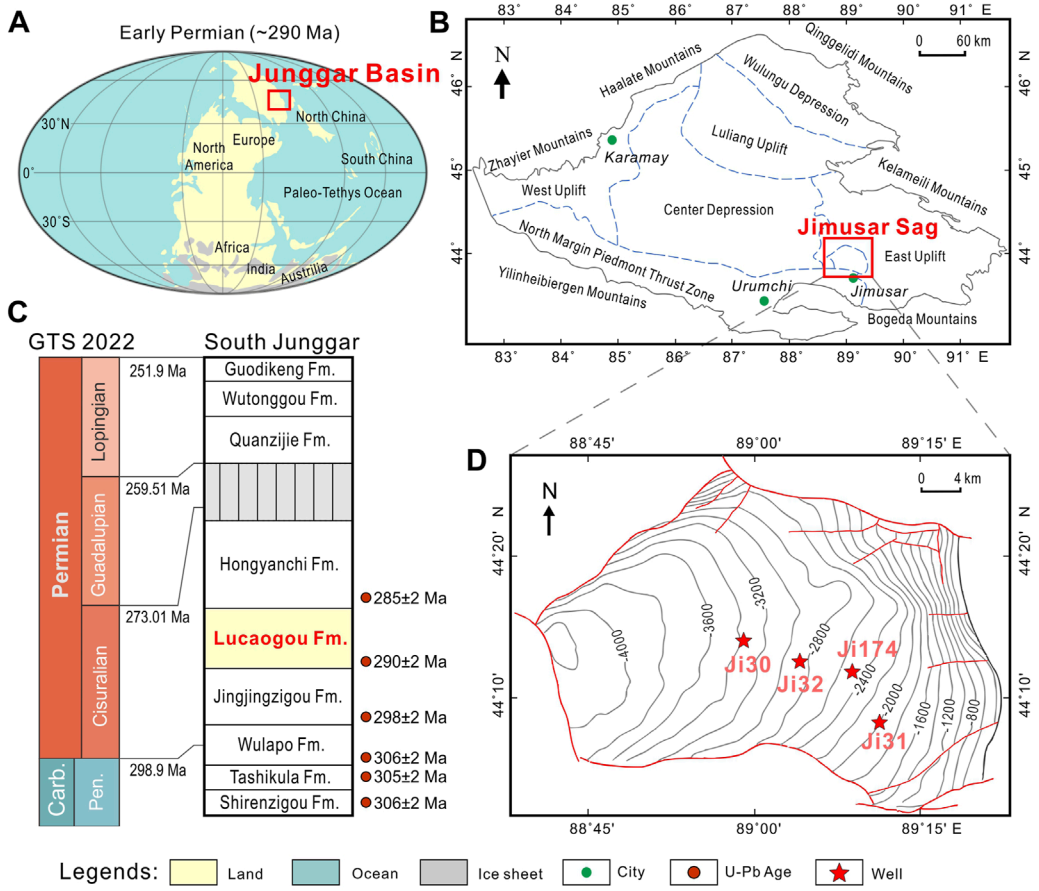

FIGURE 1
Overview of Jimusar Sag in Junggar Basin. **(A)** The Early Permian (~290 Ma) paleogeography and the location of the Junggar Basin (modified from Sun et al. (2022)), the pale yellow area, blue area and light gray area represent the land, ocean and ice cap respectively. **(B)** Location of Jimusar Sag and Ji174 well in the Junggar Basin. **(C)** The Permian age framework of South Junggar Basin (modified from Tang et al. (2022)). **(D)** Structure contour map of the Permian Lucaogou Formation and location of wells Ji30, Ji32, Ji174, and Ji31 in the Jimusar Sag (modified from Hu et al. (2017)).

the Carboniferous to the Permian, the basin experienced a transition from marine to terrestrial depositional settings (Bian et al., 2010; Gao et al., 2020). During the Permian, two hydrocarbon source rock and oil-bearing layers, namely, the Fengcheng Formation and the Lucaogou Formation, were formed in the basin (Hu et al., 2017; Cao et al., 2020).

The Jimusar Sag is located in the eastern zone of the Junggar Basin, covering an area of about 1,200 km^2. It is a sag with a deeper western side, formed in the Upper Carboniferous basement (Figure 1D), with sharp external boundarys (Su, 2019; Zhang et al., 2021; Wang et al., 2022). During the early Permian, a series of lacustrine sedimentary rock were deposited, giving rise to the important hydrocarbon source rock in the region, the Lucaogou Formation. The maximum thickness of the Lucaogou Formation is approximately 400 m, with a typical thickness ranging from 200 to 350 m. The Lucaogou Formation is mainly located in the eastern part of the Junggar Basin, and is conformable contact with the overlying Hongyanchi Formation and the underlying Jingjingzigou Formation (Figure 1C) (Tang et al., 2022). The lithology is mostly fine-grained sedimentary rocks, mainly shale, mudstone, siltstone and fine sandstone, with interbedded limestone and dolomite. The depositional environment of the Lucaogou Formation is lacustrine, where the shales may represent deeper periods in the lake basin, while the sandstones and siltstones may indicate shallower periods in the basin (Qiu et al., 2017).

Considering the recent advancements in the chronology research of the Lucaogou Formation in 2022 (Sun et al., 2022; Tang et al., 2022), an age of ~290 Ma appears to be more appropriate. Gao et al. (2020) obtained a maximum depositional age of 269 Ma based on published radiometric dating of volcanic zircons and detrital zircons. Considering biostratigraphy (*Anthraconauta–Pseudomodiolus–Mrassiella* bivalve assemblage), they suggest that the Lucaogou Formation belongs to the Guadalupian, with a more specific age range of approximately 268–270 Ma (Huang et al., 2020). Sun et al. (2022) performed CA-ID-TIMS dating of volcanic ash in the upper part of the Lucaogou Formation in the Jingjingzigou section, southern Junggar Basin and obtained a result of 286.39 ± 0.25 Ma. LA-ICP-MS dating of tuffaceous siltstone in the top of the underlying Jingjingzigou Formation resulted in 294.1 ± 1.4 Ma. Tang et al. (2022) summarized published chronostratigraphic and biostratigraphic results, combining detrital zircon ages and biostratigraphic data, and

assigned the Lucaogou Formation to the Cisuralian, with the lower boundary constrained to 290 ± 2 Ma. Additionally, on the western margin of the Turpan-Hami Basin, Yang et al. (2010) conducted CA-ID-TIMS U-Pb dating on volcanic ashes near the upper boundary of the Hongyanchi Formation, obtaining an age of 281.39 ± 0.10 Ma. They assigned both the Hongyanchi Formation and the Lucaogou Formation to the Cisuralian. In this study, we adopt the CA-ID-TIMS zircon U-Pb dating result of Sun et al. (2022) that the Lucaogou Formation was deposited about 290 Ma, and the 269 Ma previously obtained by Liu et al. (2017) may have been influenced by Pb loss in a single detrital zircon, leading to a biased younger age estimation.

3 Data and methods

3.1 GR logging and TOC data series

Natural gamma ray (GR) logging data can be used as paleoclimate proxy in cyclostratigraphy studies (Wu et al., 2009; Wu et al., 2013; Huang and Hinnov, 2019). This data measures the intensity of gamma rays emitted during the decay of radioactive substances (such as U, Th, K) in rocks, reflecting the abundance of radioactive components in the rocks. Clay minerals have fine grain size, often slow settling rate, and a tendency to adsorb radioactive elements (U and Th). K is also one of the constituent elements of illite. Shale is often rich in clay minerals and organic matter (Wu et al., 2008). Therefore, in sedimentary rocks, sandstones, conglomerates, and carbonates generally exhibit lower GR logging values, while shale exhibits higher GR logging values. Thus, GR logging values can clearly reflect lithological variations. In sedimentary basins, lithological changes can indicate fluctuations in lake levels, river input capacity, and continental weathering intensity, all of which are closely related to paleoclimate changes controlled by hydrological cycles. Total organic carbon (TOC) is the carbon present in rocks as organic matter. Additionally, numerous cases have been reported where Milankovitch cycles were identified based on TOC data (Melles et al., 2012; Liu et al., 2014; Huang et al., 2021). TOC values can reflect the water chemistry, initial productivity, and preservation conditions of the basin. These factors collectively represent carbon burial, which is an important component of the Earth's carbon cycle.

We conducted cyclostratigraphic studies on four wells from the Lucaogou Formation in the Jimusar Sag. For wells Ji30, Ji31, and Ji32, we investigated GR logging data series (Figure 2). For well Ji174, we collected both GR logging and TOC data series. The high-resolution GR logging data series for the four wells were obtained from Huang et al. (2020), with an original sampling interval of 0.125 m, covering the entire Lucaogou Formation. Most GR logging data values fluctuate frequently in the range of 50–150 API (Figure 2). Among them, Ji30, Ji31, and Ji32 wells exhibit some high values exceeding 200 API, which may be attributed to the lithology being carbonate during logging. Based on these high-frequency fluctuations, spectral analysis is deemed necessary.

The TOC data series for well Ji174 were sourced from Hu et al. (2017) and comprised measurements from 265 lacustrine shale samples. The 265 TOC data points from well Ji174 range between 0.27 and 19.01, with a mean of 3.557. Generally, the upper and lower parts of the Lucaogou Formation often exhibit high TOC values, while the middle part tends to have lower TOC values (Figure 2). High-frequency fluctuation characteristics also appear in the TOC data series. The TOC data series does not cover the entire Lucaogou Formation, with a missing interval from 3104 to 3109.22 m, and lower sampling resolution after 3338.1 m, which may affect the identification of 10 kyr-scale cycles. Therefore, we selected the TOC data interval from 3109.22 to 3338.10 m, with an average sampling interval of 0.785 m.

According to the Nyquist frequency, at least two data points are needed to identify a complete cycle. The optimal sampling density is having four data points within one cycle. This ensures efficient data collection without wasting time and resources while capturing the true and complete signal (Kodama and Hinnov, 2014). Previous studies of the Lucaogou Formation have indicated a sedimentation rate of approximately 9–10 cm/kyr (Huang et al., 2020), suggesting that a precession cycle of ~18 kyr corresponds to a cycle of approximately 1.6–1.8 m in depth domain. Therefore, a minimum sampling interval of 0.8 m is required to capture these precession-scale cycles. The GR logging data series has a sampling interval of 0.125 m, enabling the identification of cycles with a minimum period of 0.25 m. The average sampling interval for the TOC data series is 0.785 m, allowing the identification of cycles with a minimum period of 1.5 m. Thus, the resolution of all five data series is sufficient to detect the orbital cycles.

3.2 Spectral analysis

3.2.1 Astronomical target frequencies at 290 Ma

Combining the previous results (Sun et al., 2022), we suggest that the age of the Lucaogou Formation is ~290 Ma. We select 290 Ma as the median age of the Lucaogou Formation and combine the astronomical solutions from La04 (Laskar et al., 2004), Berger et al. (1992) and W15 (Waltham, 2015) to obtain the astronomical target frequencies. The eccentricity cycles are derived from the widely used La04 orbital solution (Laskar et al., 2004). With the exception of the stable eccentricity cycle (405 kyr, ~100 kyr), the obliquity and precession cycles are shorter and have been changing over the geological time. The obliquity cycles are based on the theoretical calculations predicted within 500 Ma by Berger et al. (1992). In the "Astrochron" package (Meyers, 2014), you can conveniently obtain the obliquity cycles using the "bergerPeriods" function. The precession cycles are based on W15 tidal model (Waltham, 2015), that can be directly obtained from the "Milankovitch Calculator" (Waltham, 2015, available at: https://davidwaltham.com/wp-content/uploads/2014/01/Milankovitch.html). Furthermore, these predicted obliquity and precession cycles can also be directly obtained in "COCO" of Acycle software. At 290 Ma, the periods of the dominant components have been estimated as 43.3 kyr (O1) and 34.5 kyr (O2) for obliquity and 21.8 kyr (P1), 20.7 kyr (P2) and 17.7 kyr (P3) for precession. Therefore, the application of Milankovitch cycles in this study are 405 kyr for long eccentricity, 100 kyr for short eccentricity, 43.3 kyr and 34.5 kyr for obliquity and 21.8 kyr, 20.7 kyr and 17.7 kyr for precession. The ratio of E: e: O1: O2: P1: P2: P3 is about 22.88: 5.65: 2.45: 1.95: 1.23: 1.17: 1.

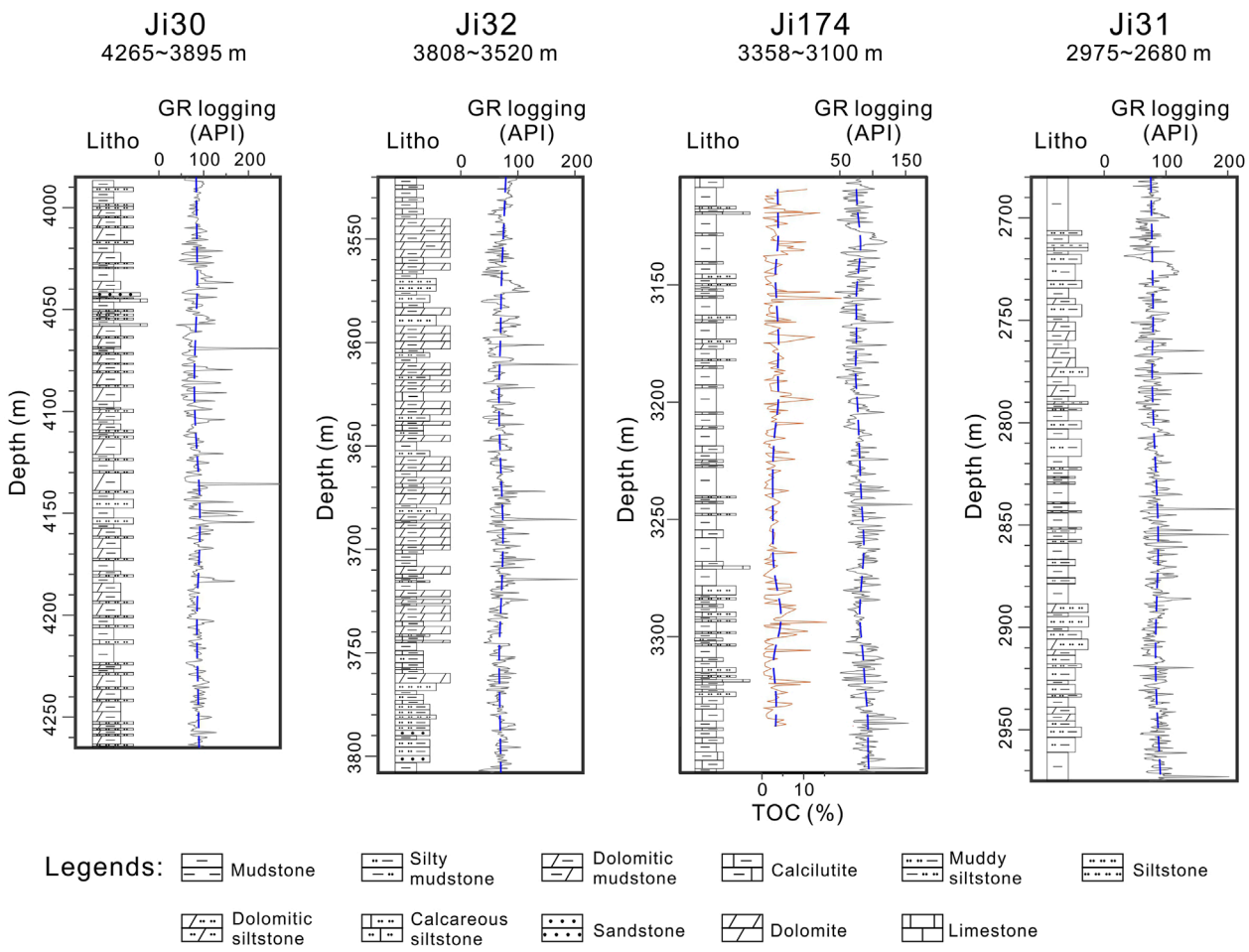

FIGURE 2
GR logging and TOC raw data series of Lucaogou Formation in wells Ji30, Ji32, Ji174 and Ji31. The lithological columns modified from Su (2019). The blue dotted lines in GR logging and TOC series are long-period trend lines that do not belong to the scale of orbital cycles.

3.2.2 Procedure of spectral analysis

We used the "Astrochron" package in R (Meyers, 2014) and Acycle software (Li et al., 2019) for the spectral analysis. Here are some key steps for data processing and analysis. First, all data series were detrended using the "Detrending" in Acycle Software to remove long-term trends that do not belong to the Milankovitch cycle bands. Next, the extreme values in the data series were removed use "remove peaks" in Acycle software to get better results in spectra. Finally, the data series are interpolated at equally spacing of 0.125 m to obtain data series that is favorable for capturing the signal at the Milankovitch cycles scale.

Spectral analysis was performed with the widely utilized multi-taper method (MTM, Thomson, 1982) in conjunction with the Robust AR (1) noise model (Mann and Lees, 1996). The MTM analysis allows us to obtain the average spectral signal of data series. The EHA spectral analysis was conducted to assess the variation of the spectrum changes with depth (or time). Select the default method of Fast Fourier transform (LAH) by Linda A. Hinnov (Kodama and Hinnov, 2015) in the Acycle software. The confidence level of the frequency domain signals can be quantified by 90%, 95%, and 99% confidence curves. The ratio relationship of each peak in the spectra (e.g., 405: 100: 43.3: 34.5: 21.8: 20.7: 17.7 ≈ 22.88: 5.65: 2.45: 1.95: 1.23: 1.17: 1) and the deposition rate results of COCO are combined to determine the present of astronomical cycles.

After obtaining the spectra of data series, the COCO (Correlation Coefficient) was used to estimate the sedimentation rate. This technique estimates the product-moment correlation coefficient between the power spectra of astronomical solutions and paleoclimate proxy series across a range of test sedimentation rates. The number of contributing astronomical parameters in the estimate is also considered. Based on the astronomical target frequencies we selected, we can evaluate the optimal sedimentation rate by observing the joint maxima of correlation coefficients (rho) and null hypothesis test (H_0-SL) in the COCO results.

The high confidence level signals within the depth domain data series are subjected to Gaussian filtering, and the depth domain data is tuned to the time domain based on the corresponding astronomical target cycles to establish a floating ATS. Subsequently, the signal bands representing obliquity in each data series are filtered using the Hilbert transform to obtain the AM series of the obliquity. The obtained AM series is further analyzed using MTM spectral analysis to capture the AM cycle frequency.

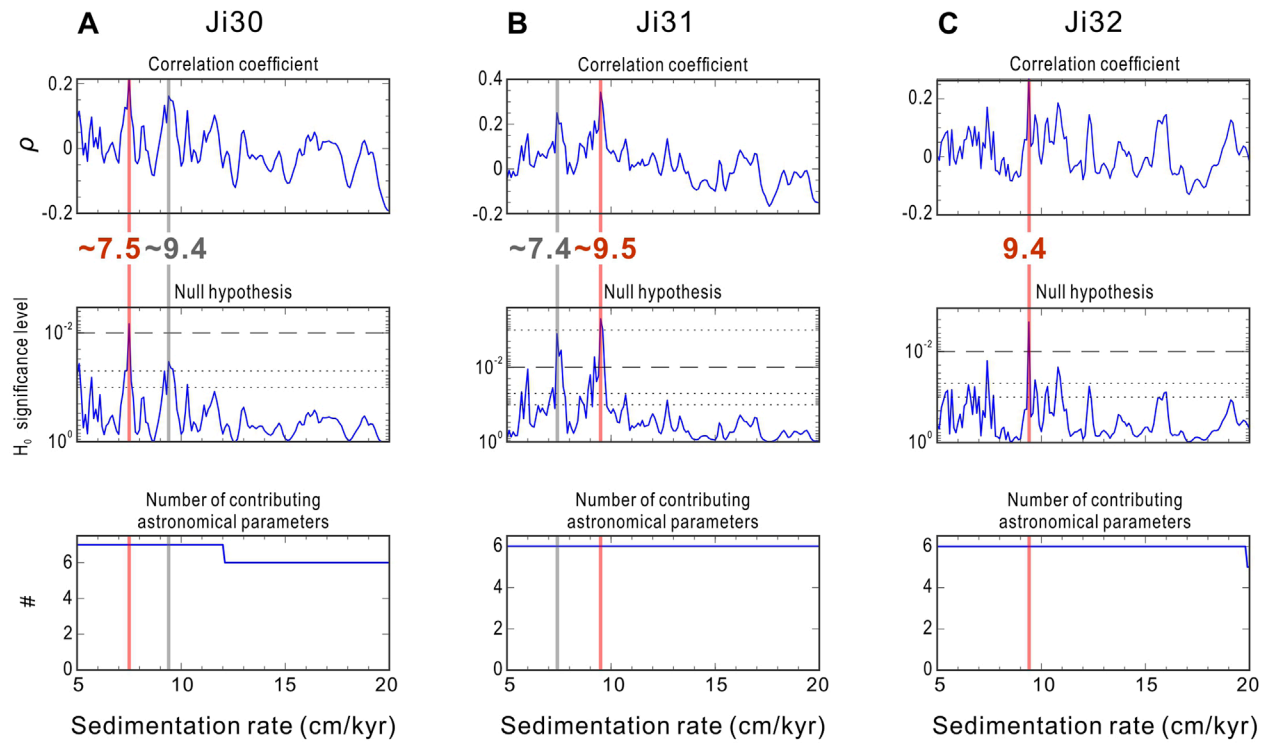

FIGURE 3
COCO analysis results of detrended GR logging series from well Ji30, Ji31 and Ji32 in the stratigraphic domain. The target astronomical series are from La04 (Laskar et al., 2004), Berger et al. (1992) and W15 (Waltham, 2015) solutions at 290 Ma. The number of Monte Carlo simulations is 4000. Sedimentation rates range from 0 to 20 cm/kyr with a step of 0.1 cm/kyr. **(A)** The rho and H_0-SL results of Ji30 GR logging data series. **(B)** The rho and H_0-SL results of Ji31 GR logging data series. **(C)** The rho and H_0-SL results of Ji32 GR logging data series.

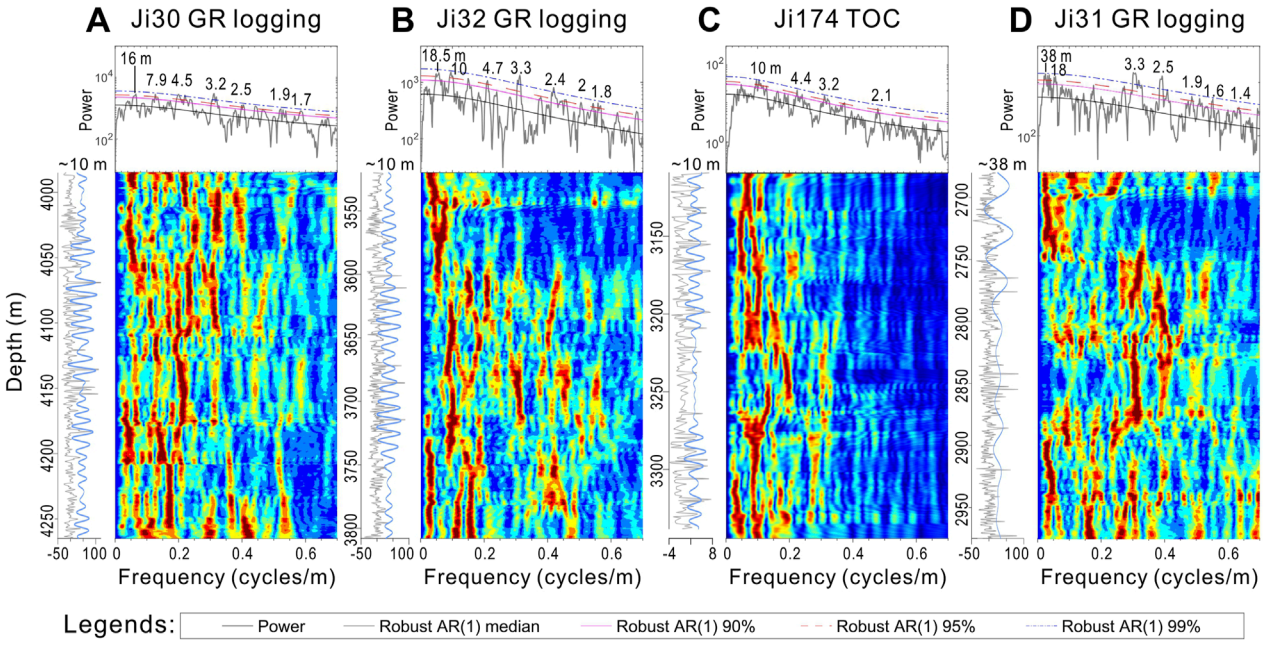

FIGURE 4
Spectral analysis results of detrended GR logging and TOC series from wells Ji30, Ji32, Ji174 and Ji31 in the depth domain. The blue curve represents the eccentricity signal extracted from data series. **(A)** 2π MTM power spectrum and evolutive harmonic analysis (EHA) results of Ji30 GR logging data series. **(B)** 2π MTM power spectrum and evolutive harmonic analysis (EHA) results of Ji32GR logging data series. **(C)** 2π MTM power spectrum and evolutive harmonic analysis (EHA) results of Ji174 TOC data series. **(D)** 2π MTM power spectrum and evolutive harmonic analysis (EHA) results of Ji31 GR logging data series.

4 Results

4.1 Cyclostratigraphic analysis in the depth domain

The detrended data series from the four wells were subjected to MTM spectral analysis after applying the "Detrending" and "Remove Peaks" functions in the Acycle software. Using "LOWESS" method to remove 35% weighted average in Acycle software. This analysis revealed a series of high confidence level peaks in frequency domain. In Ji30 well, cycles with wavelengths of 16 m, 7.9 m, 4.5 m, 3.2 m, 2.5 m, 1.9 m, and 1.7 m above the 95% confidence level. In Ji31 well, cycles with wavelengths of 38 m, 18 m, 3.3 m, 2.5 m, 1.9 m, and 1.6 m above the 95% confidence level. In Ji32 well, cycles with wavelengths of 18.5 m, 10 m, 4.7 m, 3.3 m, 2.4 m, 2 m, and 1.8 m above the 95% confidence level. Consistent with previous results (Li et al., 2018), in Ji174 well, detrended TOC data series exhibited a cycle with a wavelength of ~10 m above the 99% confidence level, and cycles with wavelengths of 4.4 m, 3.2 m, and 2.1 m above the 95% confidence level. The ratios of these sedimentary cycle signals were highly consistent with the theoretical astronomical target frequencies ratios of the Early Permian (E: e: O1: O2: P1: P2: P3 ≈ 23.96: 5.92: 2.56: 2.04: 1.2: 1.14: 1). Therefore, these sedimentary cycles may represent the astronomical cycles of E (~38 m), e (~10 m), O1 (~4.5 m), O2 (~3.3 m), P1 (2.1 m), P2 (1.9 m), and P3 (1.7 m), respectively.

The optimal average sedimentation rates are estimated using the COCO method, with the removal of the red noise model set to classical AR1 in the Acycle software. The tested range of sedimentation rates is 5–20 cm/kyr, with a step of 0.1, and the astronomical target frequencies are the seven astronomical cycles determined in the previous section. The default Pearson method is used for correlation calculations, and 4000 Monte Carlo simulations are performed. The results of rho and H_0-SL both show peaks at 7.5 and 9.4 cm/kyr in the GR logging data series from Ji30, and peak at 7.4 and 9.5 cm/kyr in the GR logging data series from Ji31. In the GR logging data series from Ji32, there is a peak at 9.4 cm/kyr. The number of astronomical cycles that constrain these high confidence level peaks is more than six (Figure 3). The sedimentation rate of Ji174 has been estimated in previous studies (~9.1 cm/kyr) (Huang et al., 2020). Considering that terrestrial basins generally have higher sedimentation rates and there are no apparent sedimentary gaps in the Lucaogou Formation, we suggest an average sedimentation rate ranging from 7.4 cm/kyr to 9.5 cm/kyr for the Lucaogou Formation, which is basically consistent with previous results.

4.2 Spectral analysis in the time domain

Based on the results of the above depth domain cyclostratigraphic analysis, we conclude that the deposition process of the Lucaogou Formation was influenced by astronomical signals, where the ~38 m and ~10 m cycles represent the long and short eccentricity signals, respectively. Since eccentricity signals have remained stable throughout geological times, we selected the long eccentricity signal (405 kyr) for astronomical tuning of the depth domain series in well Ji31, and the short eccentricity signal (~100 kyr) for astronomical tuning of the depth domain series in wells Ji30, Ji32, and Ji174. For well Ji31, we selected the ~38 m band for Gaussian filtering, and the results showed 8 peaks (Figure 4), representing 7 complete 405 kyr cycles; for wells Ji30, Ji32, and Ji174, we selected the ~10 m band for Gaussian filtering, and the filtering results showed 28–30 peaks (Figure 4), representing 27–29 complete ~100 kyr cycles (due to well Ji174 is partially missing at the top and base, there are only 26 peaks, or 25 complete ~100 kyr cycles). By assigning a time scale of 100 kyr (or 405 kyr) to each sedimentary cycle, the duration of these four wells in the Lucaogou Formation can be obtained separately. Previous work found that the eccentricity signal was missing in the GR logging data series of well Ji174, and we chose to use the TOC data series for astronomical tuning and applied the resulting floating ATS to the GR logging data series. Both TOC and GR logging data series were subjected to the cyclostratigraphic analysis of time domain.

In the time domain, the 2π-MTM spectral analysis and EHA spectral analysis were conducted. The results show that in the series from well Ji30, the short eccentricity signal (100 kyr), obliquity band signals (45.2 kyr, 36.7 kyr), and precession band signal (21.4 kyr) exceeded the 95% confidence level (Figure 5). In the series from well Ji31, the long eccentricity signal (405 kyr), obliquity band signals (38.7 kyr, 32.6 kyr), precession band signals (22 kyr, 19.7 kyr, 17.3 kyr), and signals in the range of 200–170 kyr exceeded the 95% confidence level (Figure 5). In the series from well Ji32, the short eccentricity signal (100 kyr), obliquity band signals (50 kyr, 31.6 kyr), precession band signals (19.2 kyr, 17 kyr), and signals in the range of 200–170 kyr exceeded the 95% confidence level (Figure 5). The TOC data from well Ji174 exhibited a short eccentricity cycle (~100 kyr), obliquity signals from 48 to 28.8 kyr, and precession cycles of 22 kyr and 19.8 kyr. The GR logging data showed obliquity signals from 42.9 to 34.5 kyr and precession cycles of 21.1 kyr and 18 kyr (Figure 5).

Combining the theoretical astronomical target frequencies in Early Permian, we suggest that the four wells preserved astronomical cycles, while their different astronomical cycle patterns may stem from the differences of well locations and complexity of sedimentary processes. It is worth noting that in addition to the eccentricity, obliquity and precession cycles, a signal with a period of ~170 kyr has been observed in wells Ji31, Ji32, and Ji174. By extracting this ~170 kyr signal from the detrended GR logging and TOC time series (Figure 6), we can find that this ~170 kyr cycle may have influenced the fluctuations in TOC and GR logging data. To determine the origin of this signal, the obliquity band signals were extracted from the GR logging and TOC time series of the Lucaogou Formation in the four wells, afterwards applied Hilbert transform on the obliquity signal curves to obtain their AM series. MTM spectral analysis was then conducted on the obliquity AM series, consistently showing a high confidence level s_3-s_6 obliquity AM cycle with a wavelength of ~170 kyr. This ~170 kyr cycle is in close proximity to the obliquity modulation cycles identified in previous studies of marine sedimentary records (Boulila et al., 2018). Therefore, it is suggested that the GR logging and TOC data from the four wells in the Lucaogou Formation of the Junggar Basin may record the signal of this obliquity AM cycle.

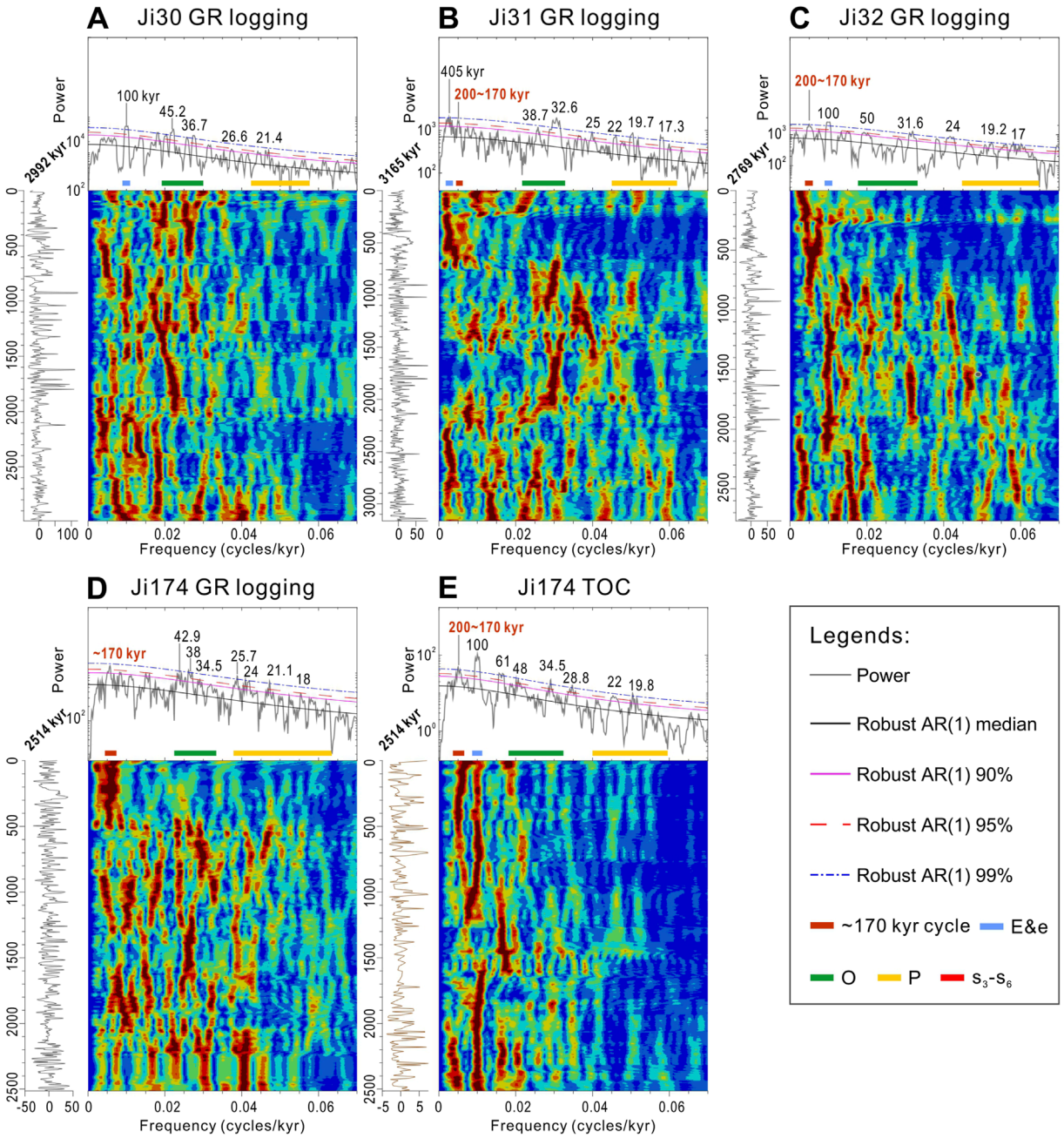

FIGURE 5
Spectral analysis results of GR logging (Ji30, Ji31, Ji32 and Ji174) and TOC(Ji174) time series. **(A–E)** 2π MTM power spectrum and evolutive harmonic analysis (EHA) results of Ji30 GR logging time series, Ji31 GR logging time series, Ji32 GR logging time series, Ji174 GR logging time series and Ji174 TOC time series.

5 Discussion

5.1 Duration and sedimentation rate of the Lucaogou Formation

Based on previous chronology studies, the sedimentary age of the Lucaogou Formation is ~290 Ma, belong to Cisuralian. Astronomical target frequencies we choosed are E (405 kyr), e (100 kyr), o1 (43.3 kyr), o2 (34.5 kyr), p1 (21.8 kyr), p2 (20.7 kyr) and p3 (17.7 kyr). In these wells, the depth interval of the Lucaogou Formation is about 250 m. This depth range is too short to cut data series into several parts, then tuning respectively. Therefore, we choose to apply filtering and tuning directly to the entire data series. We choose to establish floating ATSs using eccentricity cycles (405 kyr and ~100 kyr) that have remained stable during the geological times. The 405 kyr long eccentricity cycle was used in Ji31 well and the ~100 kyr short eccentricity cycle was used in Ji30, Ji32 and Ji174 well. The lack of long eccentricity cycle in Ji30, Ji32 and Ji174 well may be attributed to different positions in sedimentary system due to differences in well locations.

10.3389/feart.2024.1272857

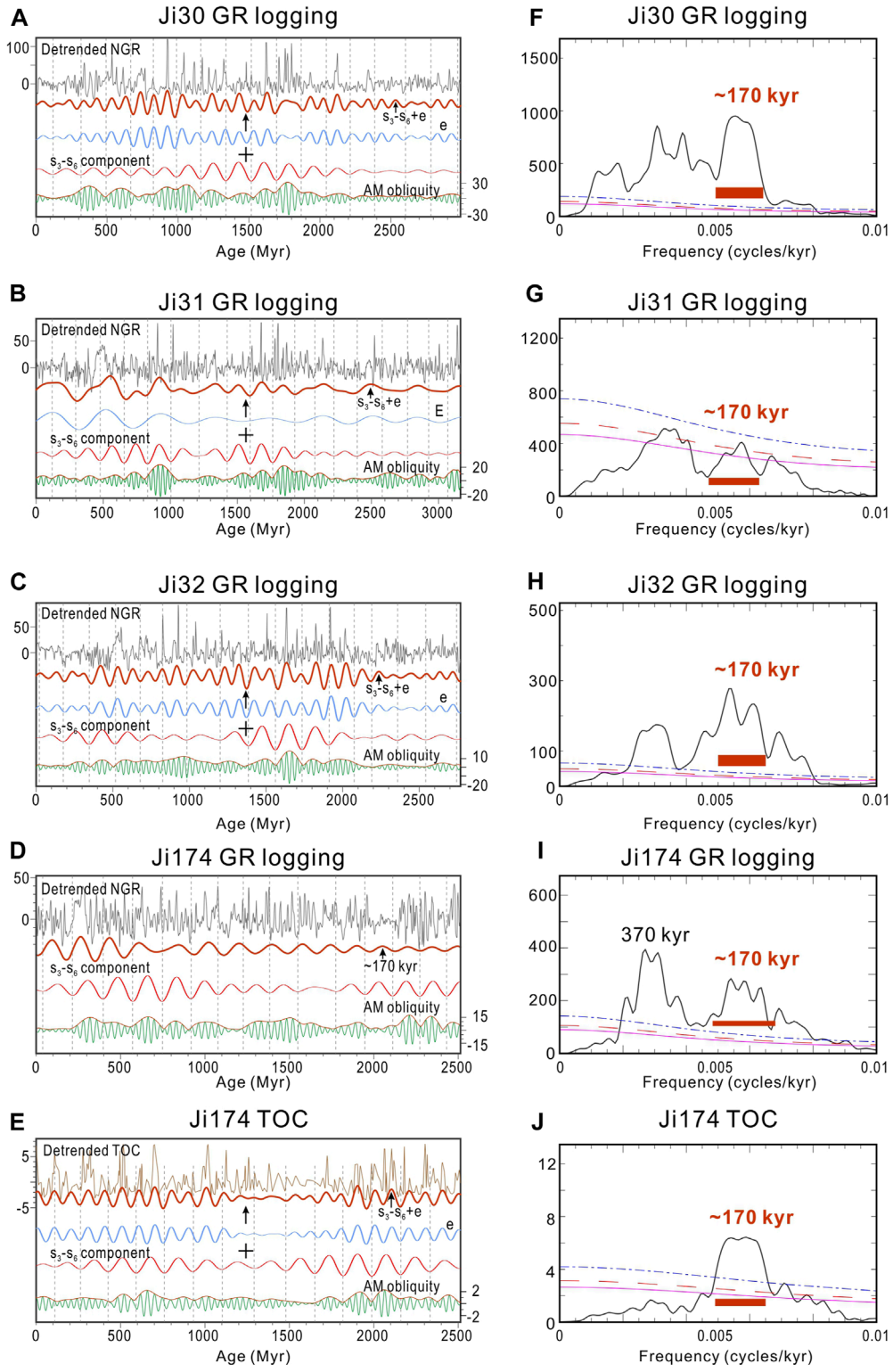

FIGURE 6
Spectral analysis of the detrended GR logging (Ji30, Ji31, Ji32 and Ji174) and TOC (Ji174) obliquity AM series. The green curves represent obliquity signals extracted from the detrended time series (with a bandpass of 0.026 ± 0.006 cycles/kyr). The red curves represent the s_3-s_6 obliquity AM cycles extracted from the obliquity AM series (with a bandpass of 0.0058 ± 0.001 cycles/kyr). The blue curves represent eccentricity cycles extracted from the detrended time series (long eccentricity cycles with a bandpass of 0.025 ± 0.005 cycles/kyr, short eccentricity cycles with a bandpass of 0.01 ± 0.002 cycles/kyr). **(A–E)** The eccentricity, obliquity and s_3-s_6 obliquity AM cycles in Ji30 GR logging, Ji31 GR logging, Ji32 GR logging, Ji174 GR logging and Ji174 TOC time series. **(F–J)** 2π MTM power spectrum analysis of the detrended GR logging (Ji30, Ji31, Ji32 and Ji174) and TOC (Ji174) obliquity AM series.

Huang et al. (2020) conducted a comprehensive cyclostratigraphic analysis of the GR logging data from five wells in the Lucaogou Formation. Based on the Ji251 well, which recorded a long eccentricity cycle of 405 kyr, they provided sedimentation rates ranging from 8.9 to 10.3 cm/kyr. In this study, COCO results exhibit a combined peak of rho and H_0-SL at 9.4 cm/kyr in Ji32 well (Figure 3). However, in Ji30 and Ji31 wells, combined peaks appear at ~7.5 cm/kyr and ~9.5 cm/kyr, respectively (Figure 3). This may indicate variations in sedimentation rates during the deposition of the Lucaogou Formation. Two organic matter rich intervals were formed in the Lucaogou Formation, predominantly composed of mudstone, silty mudstone and dolomitic mudstone. Conversely, siltstone and carbonate rocks are more prevalent in other intervals with relatively low TOC content (Su, 2019). These changes in TOC content and lithology may signify fluctuation in climate and sedimentary systems, leading to the occurrence of two peaks in COCO results of Ji30 and Ji31 wells. Nevertheless, the Lucaogou Formation has consistently been interpreted as lacustrine, with lithological columns showing no significant sedimentary interruptions (Figure 2), indicating that there is no strong change in sedimentation rate. Therefore, we choose to provide the average sedimentation rate of the Lucaogou Formation, which ranges approximately from 7.5 to 9.5 cm/kyr. This result falls within the common range of sedimentation rates for lacustrine fine-grained sedimentary rocks (Huang et al., 2021; Zhang R. et al., 2022; Wu et al., 2022) and is consistent with previous results (Carroll and Wartes, 2003; Huang et al., 2020).

Previous astronomical tuning resulted in a sedimentation duration of 3 ± 0.2 Myr for the Lucaogou Formation (Huang et al., 2020). After Gaussian filtering and astronomical tuning using the eccentricity signal, floating ATSs for wells Ji30, Ji31, and Ji32 are estimated to be 2992 kyr, 3165 kyr, and 2769 kyr, respectively. In general, the error range of astronomical tuning is the result plus or minus one period of tuning signal (Meyers et al., 2012; Sageman et al., 2014; Ma and Li, 2020), so the results and error ranges of wells Ji30, Ji31, and Ji32 are 2992 ± 100 kyr, 3165 ± 405 kyr, and 2769 ± 100 kyr, respectively. Considering that the floating ATS of well Ji174 established with short eccentricity signal in our previous work lasts for about 2.8 Myr, we suggest that the duration of the Lucaogou Formation ranges from 2.8 to 3.2 Myr and the variation depends on the depositional position, which is consistent with the previous results (Huang et al., 2020).

The data series from the four wells also contain strong obliquity band signals in addition to the eccentricity signals. We previously attempted to filter and tune the Lucaogou Formation in well Ji174 using obliquity bands and obliquity AM cycle (s_3-s_6), and the results were all in the range of ~2.8 Myr, consistent to the tuning results of the short eccentricity signal. This may indicate the feasibility of applying the ~170 kyr cycle to astronomical tuning of Paleozoic strata.

5.2 The ~170 kyr cycle in the Lucaogou Formation

According to theoretical astronomical solutions, the ~170 kyr cycle can be attributed to the inclination cycle of the Earth's orbit or to the obliquity AM cycle (s_3-s_6) (Huang et al., 2021). The inclination of the Earth's orbit is the angle between the Earth's orbit and the plane of the solar system (Hinnov, 2000). However, the variation of the mean total solar radiation caused by the periodic variation of the orbital inclination is very small, three orders of magnitude different from the variation of the mean total solar radiation caused by the eccentricity (Vieira et al., 2012). Therefore, the contribution of the orbital inclination is too weak and is difficult to be recorded in paleoclimate indicators. Since the Lucaogou Formation exhibits strong obliquity signals, and the spectral analysis of the obliquity AM series consistently shows a high confidence level ~170 kyr cycle, we suggest that the ~170 kyr cycle observed in four wells of this study might originate from the obliquity AM cycle s_3-s_6 (corresponding to the Earth and Saturn's nodal precession, approximately 173 kyr), which originates from the gravitational interaction between the Earth and Saturn (Boulila et al., 2018).

However, this s_3-s_6 cycle belong to the theoretically low-AM cycles (e.g., ~9 Myr, ~2.4 Myr, ~1.2 Myr, ~400 kyr, and ~170 kyr in this study), which typically do not directly appear in geological records. Instead, they are often discovered in the AM series of eccentricity, obliquity, and precession. The s_3-s_6 a.m. cycle can only explain the high confidence level ~170 kyr signal in the obliquity AM series, but should not be obviously present in the detrended GR logging and TOC data series of time domain.

Previous studies suggest that these AM cycles can be manifested through nonlinear response feedbacks between external orbital forcing and the internal climate and sedimentary systems (Martinez and Dera, 2015; Storm et al., 2020). Nonlinear features are common in the Earth's climate and depositional system. The Earth's climate system encompasses numerous complex processes, many of which exhibit nonlinear characteristics, such as "threshold" effects, abrupt events, and chaotic behavior (Rial et al., 2004). Thus, external orbital forcings can manifest in geological records after passing through a series of positive and negative feedbacks and multiple equilibria.

Additionally, recent climate modeling studies also support these nonlinear features. Caccamo and Magazù (2023) conducted comparative Wavelet-Fourier analysis on reconstructed temperature records, discussing exponential feedback effects in a climate parametric resonance model. They found exponential amplification of temperature changes from interglacial to glacial periods, demonstrating that external orbital forcings provide energy to the climate system through a series of connected resonances. Additionally, numerical simulation results based on climate stochastic resonance model (Palmer, 2019) indicate that an increase of the Earth temperature boosts a transition towards a chaotic regime where the Milankovitch cycle effects disappear. These findings demonstrate the threshold effect, wherein even small temperature increase can have significant impacts above a given threshold (Caccamo and Magazù, 2021).

Huang et al. (2021) have proposed that "Obliquity threshold response model". In this model, the ~170 kyr AM cycle is enhanced in a scenario of obliquity forcing across a geochemical "threshold" within sedimentary basins. This "threshold" can be the equilibrium of the lake biogeochemistry, which is a considerable tipping point capable of clipping the obliquity signal. Here, we can use this

"Obliquity threshold response model" and suggest that the ~170 kyr signal in the detrended GR logging and TOC time series may arise from the nonlinear characteristics of the Earth's climate system. Specifically, we propose that the biochemical equilibrium of the lake acts as a "threshold" to amplify the AM cycle (~170 kyr cycle) and record them in the GR logging and TOC series (Raymo and Nisancioglu, 2003; Huybers, 2006).

Some Paleozoic cyclostratigraphic studies have investigated AM cycles, but most of these studies have focused on long AM cycles at the million-year scale, such as the s_4-s_3 obliquity AM cycle and the g_4-g_3 eccentricity AM cycle (Zhao et al., 2022). The ~170 kyr cycle has been identified in marine records, but its interpretation and origin have not been extensively explored (De Vleeschouwer et al., 2013; Zhong et al., 2020). In terrestrial strata, Huang et al. (2020) identified a cycle of 16.5–19.3 m in five wells in the Junggar Basin and suggested that it may originate from the obliquity AM cycle s_3-s_6, but no further analysis was conducted on the obliquity AM series. Here, we further identified the ~170 kyr cycle in all four wells in the Jimusar Sag of the Junggar Basin and confirmed the existence of this cycle at different locations in the sag.

5.3 Astronomical cycles regulate the sedimentary system of an Early Permian terrestrial basin

During the Early Permian, the Junggar Basin was located in the mid-high latitude regions of the Northern Hemisphere (Scotese, 2021). Obliquity can influence the latitudinal distribution of insolation, thereby impacting climate and sedimentary systems by regulating the amount of insolation received in mid-high latitude regions. To better explain how obliquity regulates terrestrial organic carbon burial during greenhouse climate periods, previous researchers have proposed "obliquity-forced organic carbon burial model" (Huang et al., 2021). The model suggests that in mid-high latitude regions, as obliquity changes, the heat, water circulation, and chemical weathering changes. These can affect lake eutrophication and bottom water conditions, thus regulating organic carbon burial. In the high value of obliquity, the mid-high latitude regions are characterized by high heat, strong hydrological cycle and chemical weathering, so the lakes are eutrophic and the bottom water is anoxic, which is conducive to the preservation of organic matter, and *vice versa*.

Here, we have identified high confidence level obliquity signals in the GR logging and TOC data series of all four wells. The lithology of the Lucaogou Formation is mainly lacustrine fine-grained sedimentary rocks. The GR logging data can indicate in mud and organic content of the rock. Considering the positive correlation between GR logging and TOC data, the GR logging data can indirectly indicate organic matter enrichment in the Lucaogou Formation. Thus, the presence of the ~170 kyr cycle, high confidence level obliquity signals, and the s_3-s_6 obliquity AM cycle in the GR logging and TOC data series of four wells supports the "obliquity-forced organic carbon burial model" and the "obliquity threshold response model," and these two models widely affects the Lucaogou Formation in the Jimusar Sag.

In addition, eccentricity signals have been consistently observed in all four wells. Therefore, we propose that eccentricity and obliquity collectively control the paleoclimatic conditions during the deposition of the Lucaogou Formation, which is ultimately reflected in the geophysical data series (GR logging) and organic carbon burial data series (TOC). When both the eccentricity signal and obliquity signal are in their crests, they combine to produce the peak values in GR logging and TOC data; whereas when they are in their troughs, the low values were recorded (Figure 6). Intermediate values are observed when one cycle is in crests while the other is in troughs (Figure 6). Eccentricity and obliquity cycles, regarded as conventional astronomical cycles, regulate paleoclimate through linear processes. Additionally, the ~170 kyr obliquity AM cycle regulated the strength of the obliquity forcing, thereby influencing the paleoclimate through a series of nonlinear processes. The superposition of the above two factors reflects the linear and nonlinear characteristics of the Earth's climate system and sedimentary processes.

6 Conclusion

The organic carbon burial and sedimentary processes of the Lucaogou Formation are influenced by eccentricity, obliquity, precession and the ~170 kyr obliquity AM cycle. High confidence level long eccentricity (405 kyr, ~38 m), short eccentricity (~100 kyr, ~10 m), obliquity band (48–33 kyr, 4.7–3.2 m), and precession band (22–18 kyr, 2.4–1.6 m) cycles were identified in the GR logging data series of wells Ji30, Ji31, Ji32, Ji174, and TOC data series of well Ji174. The number of astronomical cycles recorded varied among the wells due to differences in well locations. Based on the COCO analysis, average sedimentation rate of the Lucaogou Formation varies from ~7.5 cm/kyr to ~9.5 cm/kyr. After astronomical tuning, the sedimentation duration is about 2.8–3.2 Myr and varies according to the location of the sedimentation. Floating ATSs was established based on tunning to the eccentricity signals. Moreover, strong obliquity signals were recorded in the Lucaogou Formation. Obliquity AM series show the s_3-s_6 obliquity AM cycle (~173 kyr). Additionally, high confidence level ~170 kyr cycles were identified in TOC and GR logging time series. This ~170 kyr cycle is derived from the obliquity AM cycle. The biochemical equilibrium of the lake acts as a "threshold" to amplify the ~170 kyr cycle and record them in the GR logging and TOC series. The relationship between high GR logging and TOC values and the ~170 kyr cycle provides evidence for the obliquity-forced organic carbon burial models during the icehouse climate. The eccentricity cycle and the ~170 kyr AM cycle regulate the lacustrine sedimentary system through linear and nonlinear processes, respectively.

Data availability statement

The original contributions presented in the study are included in the article/Supplementary material, further inquiries can be directed to the corresponding author.

Author contributions

YL: Writing–original draft, Writing–review and editing. HH: Funding acquisition, Supervision, Writing–original draft, Writing–review and editing. YG: Funding acquisition, Investigation, Supervision, Writing–original draft, Writing–review and editing. YC: Writing–original draft, Writing–review and editing. HC: Writing–original draft, Writing–review and editing. CH: Writing–original draft, Writing–review and editing. SL: Writing–original draft, Writing–review and editing.

Funding

The author(s) declare that financial support was received for the research, authorship, and/or publication of this article. This study was financially supported by the National Natural Science Foundation of China (Grants No. 42302122) and the Everest Scientific Research Program of Chengdu University of Technology (Grant No. 10912-KYQD202209480).

Acknowledgments

We thank Prof. S. R. Meyers for the "astrochron" package in R. We thank Prof. Mingsong YL for the Acycle software.

Conflict of interest

The authors declare that the research was conducted in the absence of any commercial or financial relationships that could be construed as a potential conflict of interest.

Publisher's note

References

Berger, A., Loutre, M. F., and Laskar, J. (1992). Stability of the astronomical frequencies over the Earth's history for paleoclimate studies. *Science* 255 (5044), 560–566. doi:10.1126/science.255.5044.560

Bian, W., Hornung, J., Liu, Z., Wang, P., and Hinderer, M. (2010). Sedimentary and palaeoenvironmental evolution of the Junggar Basin, xinjiang, northwest China. *Palaeobiodiversity Palaeoenvironments* 90 (3), 175–186. doi:10.1007/s12549-010-0038-9

Bosmans, J. H. C., Hilgen, F. J., Tuenter, E., and Lourens, L. J. (2015). Obliquity forcing of low-latitude climate. *Clim. Past* 11 (10), 1335–1346. doi:10.5194/cp-11-1335-2015

Boulila, S., Vahlenkamp, M., De Vleeschouwer, D., Laskar, J., Yamamoto, Y., Pälike, H., et al. (2018). Towards a robust and consistent middle Eocene astronomical timescale. *Earth Planet. Sci. Lett.* 486, 94–107. doi:10.1016/j.epsl.2018.01.003

Caccamo, M. T., and Magazù, S. (2021). On the breaking of the Milankovitch cycles triggered by temperature increase: the stochastic resonance response. *Climate* 9 (4), 67. doi:10.3390/cli9040067

Caccamo, M. T., and Magazù, S. (2023). Exponential feedback effects in a parametric resonance climate model. *Sci. Rep.* 13 (1), 22984. doi:10.1038/s41598-023-50350-7

Cao, J., Xia, L., Wang, T., Zhi, D., Tang, Y., and Li, W. (2020). An alkaline lake in the Late Paleozoic Ice Age (LPIA): a review and new insights into paleoenvironment and petroleum geology. *Earth-Science Rev.* 202, 103091. doi:10.1016/j.earscirev.2020.103091

Carroll, A. R., and Wartes, M. A. (2003). Organic carbon burial by large Permian lakes, northwest China. *Special Pap. Geol. Soc. Am.* 370, 91–104. doi:10.1130/0-8137-2370-1.91

Charbonnier, G., Boulila, S., Spangenberg, J. E., Adatte, T., Föllmi, K. B., and Laskar, J. (2018). Obliquity pacing of the hydrological cycle during the oceanic anoxic event 2. *Earth Planet. Sci. Lett.* 499, 266–277. doi:10.1016/j.epsl.2018.07.029

De Vleeschouwer, D., Rakociński, M., Racki, G., Bond, D. P. G., Sobień, K., and Claeys, P. (2013). The astronomical rhythm of Late-Devonian climate change (Kowala section, Holy Cross Mountains, Poland). *Earth Planet. Sci. Lett.* 365, 25–37. doi:10.1016/j.epsl.2013.01.016

Fang, J., Wu, H., Fang, Q., Shi, M., Zhang, S., Yang, T., et al. (2020). Cyclostratigraphy of the global stratotype section and point (GSSP) of the basal Guzhangian Stage of the Cambrian Period. *Palaeogeogr. Palaeoclimatol. Palaeoecol.* 540, 109530. doi:10.1016/j.palaeo.2019.109530

Fang, Q., Wu, H., Hinnov, L. A., Wang, X., Yang, T., Li, H., et al. (2016). A record of astronomically forced climate change in a late Ordovician (Sandbian) deep marine sequence, Ordos Basin, North China. *Sediment. Geol.* 341, 163–174. doi:10.1016/j.sedgeo.2016.06.002

Fang, Q., Wu, H., Wang, X., Yang, T., Li, H., and Zhang, S. (2018). Astronomical cycles in the Serpukhovian-Moscovian (Carboniferous) marine sequence, South China and their implications for geochronology and icehouse dynamics. *J. Asian Earth Sci.* 156, 302–315. doi:10.1016/j.jseaes.2018.02.001

Fang, Q., Wu, H., Wang, X., Yang, T., Li, H., and Zhang, S. (2019). An astronomically forced cooling event during the Middle Ordovician. *Glob. Planet. Change* 173, 96–108. doi:10.1016/j.gloplacha.2018.12.010

Gambacorta, G., Menichetti, E., Trincianti, E., and Torricelli, S. (2018). Orbital control on cyclical primary productivity and benthic anoxia: astronomical tuning of the Telychian Stage (Early Silurian). *Palaeogeogr. Palaeoclimatol. Palaeoecol.* 495, 152–162. doi:10.1016/j.palaeo.2018.01.003

Gao, Y., Huang, H., Tao, H., Carroll, A. R., Qin, J., Chen, J., et al. (2020). Paleoenvironmental setting, mechanism and consequence of massive organic carbon burial in the Permian Junggar Basin, NW China. *J. Asian Earth Sci.* 194, 104222. doi:10.1016/j.jseaes.2019.104222

Hinnov, L. A. (2000). New perspectives on orbitally forced stratigraphy. *Annu. Rev. Earth Planet. Sci.* 28 (1), 419–475. doi:10.1146/annurev.earth.28.1.419

Hu, T., Pang, X., Wang, Q., Jiang, S., Wang, X., Huang, C., et al. (2017). Geochemical and geological characteristics of permian Lucaogou Formation shale of the well Ji174, jimusar sag, Junggar Basin, China: implications for shale oil exploration. *Geol. J.* 53 (5), 2371–2385. doi:10.1002/gj.3073

Huang, C., and Hinnov, L. (2019). Astronomically forced climate evolution in a saline lake record of the middle Eocene to Oligocene, Jianghan Basin, China. *Earth Planet. Sci. Lett.* 528, 115846. doi:10.1016/j.epsl.2019.115846

Huang, H., Gao, Y., Jones, M. M., Tao, H., Carroll, A. R., Ibarra, D. E., et al. (2020). Astronomical forcing of Middle Permian terrestrial climate recorded in a large paleolake in northwestern China. *Palaeogeogr. Palaeoclimatol. Palaeoecol.* 550, 109735. doi:10.1016/j.palaeo.2020.109735

Huang, H., Gao, Y., Ma, C., Jones, M. M., Zeeden, C., Ibarra, D. E., et al. (2021). Organic carbon burial is paced by a ~173-ka obliquity cycle in the middle to high latitudes. *Sci. Adv.* 7 (28), eabf9489. doi:10.1126/sciadv.abf9489

Huybers, P. (2006). Early Pleistocene glacial cycles and the integrated summer insolation forcing. *Science* 313 (5786), 508–511. doi:10.1126/science.1125249

Kodama, K. P., and Hinnov, L. A. (2014). "Time series analysis for cyclostratigraphy," in *Rock magnetic cyclostratigraphy* (John Wiley and Sons), 52–89.

Laskar, J., Robutel, P., Joutel, F., Gastineau, M., Correia, A. C. M., and Levrard, B. (2004). A long-term numerical solution for the insolation quantities of the Earth. *Astronomy Astrophysics* 428 (1), 261–285. doi:10.1051/0004-6361:20041335

Li, M., Hinnov, L., and Kump, L. (2019). Acycle: time-series analysis software for paleoclimate research and education. *Comput. Geosciences* 127, 12–22. doi:10.1016/j.cageo.2019.02.011

Li, M., Kump, L. R., Hinnov, L. A., and Mann, M. E. (2018). Tracking variable sedimentation rates and astronomical forcing in Phanerozoic paleoclimate proxy series with evolutionary correlation coefficients and hypothesis testing. *Earth Planet. Sci. Lett.* 501, 165–179. doi:10.1016/j.epsl.2018.08.041

Li, Y., Huang, H., Gao, Y., Cheng, H., Hei, C., Liang, S., et al. (2023). The 170-kyr astronomical cycles in the paleozoic terrestrial basin. *Acta Sedimentol. Sin.* 42 (1), 39–51. doi:10.14027/j.issn.1000-0550.2022.151

Liu, D., Zhang, C., Yao, E., Song, Y., Jiang, Z., and Luo, Q. (2017). What generated the Late Permian to Triassic unconformities in the southern Junggar Basin and western Turpan Basin; tectonic uplift, or increasing aridity? *Palaeogeogr. Palaeoclimatol. Palaeoecol.* 468, 1–17. doi:10.1016/j.palaeo.2016.11.045

Liu, W., Liu, Z., An, Z., Sun, J., Chang, H., Wang, N., et al. (2014). Late Miocene episodic lakes in the arid Tarim Basin, western China. *Proc. Natl. Acad. Sci.* 111 (46), 16292–16296. doi:10.1073/pnas.1410890111

Ma, C., and Li, M. (2020). Astronomical time scale of the Turonian constrained by multiple paleoclimate proxies. *Geosci. Front.* 11 (4), 1345–1352. doi:10.1016/j.gsf.2020.01.013

Ma, K., Hinnov, L. A., Zhang, X., and Gong, Y. (2020). Astronomical time calibration of the upper devonian lali section, south China. *Glob. Planet. Change* 193, 103267. doi:10.1016/j.gloplacha.2020.103267

Ma, K., Li, R., and Gong, Y. (2016). Chemostratigraphy and cyclostratigraphy of the ordovician liangjiashan section from shimenzhai of qinhuangdao in North China. *Earth Sci. Front.* 23, 268–286. doi:10.13745/j.esf.2016.06.019

Ma, K., Li, R., Hinnov, L. A., and Gong, Y. (2019). Conodont biostratigraphy and astronomical tuning of the lower–middle ordovician liangjiashan (North China) and huanghuachang (south China) marine sections. *Palaeogeogr. Palaeoclimatol. Palaeoecol.* 528, 272–287. doi:10.1016/j.palaeo.2019.05.003

Mann, M. E., and Lees, J. M. (1996). Robust estimation of background noise and signal detection in climatic time series. *Clim. Change* 33 (3), 409–445. doi:10.1007/BF00142586

Martinez, M., and Dera, G. (2015). Orbital pacing of carbon fluxes by a ~9-My eccentricity cycle during the Mesozoic. *Proc. Natl. Acad. Sci.* 112 (41), 12604–12609. doi:10.1073/pnas.1419946112

Melles, M., Brigham-Grette, J., Minyuk, P. S., Nowaczyk, N. R., Wennrich, V., DeConto, R. M., et al. (2012). 2.8 million years of Arctic climate change from Lake El'gygytgyn, NE Russia. *Science* 337 (6092), 315–320. doi:10.1126/science.1222135

Meyers, S. R. (2014). Astrochron: an R package for astrochronology. http://cran.r-project.org/package=astrochron.

Meyers, S. R., Siewert, S. E., Singer, B. S., Sageman, B. B., Condon, D. J., Obradovich, J. D., et al. (2012). Intercalibration of radioisotopic and astrochronologic time scales for the Cenomanian-Turonian boundary interval, Western Interior Basin, USA. *Geology* 40 (1), 7–10. doi:10.1130/g32261.1

Palmer, T. N. (2019). Stochastic weather and climate models. *Nat. Rev. Phys.* 1 (7), 463–471. doi:10.1038/s42254-019-0062-2

Qiu, Z., Jiang, L., and Tao, H. (2017). Characteristics of strata and depositional environment of the permian Lucaogou Formation in jimusar sag. *Chin. J. Geol.* 52 (3), 964–979. doi:10.12017/dzkx.2017.061

Raymo, M. E., and Nisancioglu, K. H. (2003). The 41 kyr world: Milankovitch's other unsolved mystery. *Paleoceanography* 18 (1), 1011. doi:10.1029/2002pa000791

Rial, J. A., Pielke, R. A., Beniston, M., Claussen, M., Canadell, J., Cox, P., et al. (2004). Nonlinearities, feedbacks and critical thresholds within the Earth's climate system. *Clim. Change* 65 (1-2), 11–38. doi:10.1023/B:CLIM.0000037493.89489.3f

Sageman, B. B., Singer, B. S., Meyers, S. R., Siewert, S. E., Walaszczyk, I., Condon, D. J., et al. (2014). Integrating 40Ar/39Ar, U-Pb, and astronomical clocks in the cretaceous niobrara formation, western interior basin, USA. *Geol. Soc. Am. Bull.* 126 (7-8), 956–973. doi:10.1130/b30929.1

Scotese, C. R. (2021). An atlas of phanerozoic paleogeographic maps: the seas Come in and the seas Go out. *Annu. Rev. Earth Planet. Sci.* 49 (1), 679–728. doi:10.1146/annurev-earth-081320-064052

Sørensen, A. L., Nielsen, A. T., Thibault, N., Zhao, Z., Schovsbo, N. H., and Dahl, T. W. (2020). Astronomically forced climate change in the late Cambrian. *Earth Planet. Sci. Lett.* 548, 116475. doi:10.1016/j.epsl.2020.116475

Storm, M. S., Hesselbo, S. P., Jenkyns, H. C., Ruhl, M., Ullmann, C. V., Xu, W., et al. (2020). Orbital pacing and secular evolution of the Early Jurassic carbon cycle. *Proc. Natl. Acad. Sci.* 117 (8), 3974–3982. doi:10.1073/pnas.1912094117

Su, Y. (2019). Processes and controlling factors of oil migration and accumulation in the tight reservoirs of the Lucaogou Formation in the jimsar sag. Junggar Basin. Doctor's thesis. Qingdao, China: China University of Petroleum.

Sun, F., Hu, W., Cao, J., Wang, X., Zhang, Z., Ramezani, J., et al. (2022). Sustained and intensified lacustrine methane cycling during Early Permian climate warming. *Nat. Commun.* 13 (1), 4856. doi:10.1038/s41467-022-32438-2

Tang, Y., Hou, Z., Wang, X., Wang, T., Wu, Q., Shen, B., et al. (2022). Progress of the carboniferous and permian stratigraphic framework and correlation of the Junggar Basin, xinjiang, northwest China. *Geol. Rev.* 68 (02), 385–407. doi:10.16509/j.georeview.2022.01.011

Thomson, D. J. (1982). Spectrum estimation and harmonic analysis. *Proc. IEEE* 70 (9), 1055–1096. doi:10.1109/PROC.1982.12433

Tian, J., Wu, H., Huang, C., Li, M., Ma, C., and Wang, P. (2022). Looking at Milankovitch theory from the 400,000-year long eccentricity period. *Earth Sci.* 47 (10), 3543–3568. doi:10.3799/dqkx.2022.248

Vieira, L. E. A., Norton, A., Dudok de Wit, T., Kretzschmar, M., Schmidt, G. A., and Cheung, M. C. M. (2012). How the inclination of Earth's orbit affects incoming solar irradiance. *Geophys. Res. Lett.* 39 (16), L16104. doi:10.1029/2012gl052950

Waltham, D. (2015). Milankovitch Period uncertainties and their impact on cyclostratigraphy. *J. Sediment. Res.* 85 (8), 990–998. doi:10.2110/jsr.2015.66

Wang, L., Ye, Y., Qin, J., Gao, Y., Deng, Y., Li, Y., et al. (2022). Microscopic pore structure characterization and oil-bearing property evaluation of lacustrine shale reservoir: a case study of the Permian Lucaogou Formation in Jimsar Sag, Junggar Basin. *Oil Gas Geol.* 43 (01), 149–160. doi:10.11743/ogg20220112

Wang, M., Chen, H., Huang, C., Kemp, D. B., Xu, T., Zhang, H., et al. (2020). Astronomical forcing and sedimentary noise modeling of lake-level changes in the Paleogene Dongpu Depression of North China. *Earth Planet. Sci. Lett.* 535, 116116. doi:10.1016/j.epsl.2020.116116

Wei, R., Zhang, R., Li, M., Wang, X., and Jin, Z. (2023). Obliquity forcing of lake-level changes and organic carbon burial during the Late Paleozoic Ice Age. *Glob. Planet. Change* 223, 104092. doi:10.1016/j.gloplacha.2023.104092

Wu, H., Fang, Q., Wang, X., Hinnov, L. A., Qi, Y., Shen, S.-z., et al. (2018). An ~34 m.y. astronomical time scale for the uppermost Mississippian through Pennsylvanian of the Carboniferous System of the Paleo-Tethyan realm. *Geology* 47 (1), 83–86. doi:10.1130/g45461.1

Wu, H., Hinnov, L. A., Zhang, S., Jiang, G., Yang, T., Li, H., et al. (2022). Continental geological evidence for solar system chaotic behavior in the late cretaceous. *Geol. Soc. Am. Bull.* 135 (3-4), 712–724. doi:10.1130/b36340.1

Wu, H., Zhang, S., Feng, Q., Fang, N., Yang, T., and Li, H. (2011). Theoretical basis, research advancement and prospects of cyclostratigraphy. *Earth Sci.* 36 (03), 409–428. doi:10.3799/dqkx.2011.045

Wu, H., Zhang, S., and Huang, Q. (2008). Establishment of floating astronomical time scale for the terrestrial late cretaceous qingshankou Formation in the Songliao Basin of northeast China. *Earth Sci. Front.* 15 (04), 159–169. doi:10.1016/S1872-5791(08)60049-4

Wu, H., Zhang, S., Jiang, G., Hinnov, L., Yang, T., Li, H., et al. (2013). Astrochronology of the early turonian–early campanian terrestrial succession in the Songliao Basin, northeastern China and its implication for long-period behavior of the solar system. *Palaeogeogr. Palaeoclimatol. Palaeoecol.* 385, 55–70. doi:10.1016/j.palaeo.2012.09.004

Wu, H., Zhang, S., Jiang, G., and Huang, Q. (2009). The floating astronomical time scale for the terrestrial Late Cretaceous Qingshankou Formation from the Songliao Basin of Northeast China and its stratigraphic and paleoclimate implications. *Earth Planet. Sci. Lett.* 278 (3-4), 308–323. doi:10.1016/j.epsl.2008.12.016

Yang, W., Feng, Q., Liu, Y., Tabor, N., Miggins, D., Crowley, J. L., et al. (2010). Depositional environments and cyclo- and chronostratigraphy of uppermost Carboniferous–Lower Triassic fluvial–lacustrine deposits, southern Bogda Mountains, NW China — a terrestrial paleoclimatic record of mid-latitude NE Pangea. *Glob. Planet. Change* 73 (1-2), 15–113. doi:10.1016/j.gloplacha.2010.03.008

Yao, X., and Hinnov, L. A. (2019). Advances in characterizing the cyclostratigraphy of binary chert-mudstone lithologic successions, permian (Roadian-lower capitanian), chaohu, lower yangtze, south China. *Palaeogeogr. Palaeoclimatol. Palaeoecol.* 528, 258–271. doi:10.1016/j.palaeo.2019.05.004

Zhang, R., Li, X., Xu, Y., Li, J., Sun, L., Yue, L., et al. (2022a). The 173-kyr obliquity cycle pacing the asian monsoon in the eastern Chinese Loess Plateau from late Miocene to Pliocene. *Geophys. Res. Lett.* 49 (2), e2021GL097008. doi:10.1029/2021gl097008

Zhang, W., Han, C., Tian, J., Zhang, Z., Zhang, N., and Li, Z. (2021). Sequence stratigraphy division and evolutionary features of permian Lucaogou Formation in jimsar sag. *Lithol. Reserv.* 33 (05), 45–58. doi:10.12108/yxyqc.20210505

Zhang, Z., Huang, Y., Li, M., Li, X., Ju, P., and Wang, C. (2022b). Obliquity-forced aquifer-eustasy during the Late Cretaceous greenhouse world. *Earth Planet. Sci. Lett.* 596, 117800. doi:10.1016/j.epsl.2022.117800

Zhao, Z., Thibault, N. R., Dahl, T. W., Schovsbo, N. H., Sorensen, A. L., Rasmussen, C. M. O., et al. (2022). Synchronizing rock clocks in the late Cambrian. *Nat. Commun.* 13 (1), 1990. doi:10.1038/s41467-022-29651-4

Zhong, Y., Wu, H., Fan, J., Fang, Q., Shi, M., Zhang, S., et al. (2020). Late ordovician obliquity-forced glacio-eustasy recorded in the yangtze block, south China. *Palaeogeogr. Palaeoclimatol. Palaeoecol.* 540, 109520. doi:10.1016/j.palaeo.2019.109520